

Strong-coupling high- T_c superconductivity in doped correlated band insulator

Yusuke Nomura,^{1,*} Motoharu Kitatani,² Shiro Sakai,³ and Ryotaro Arita^{3,4}

¹*Institute for Materials Research (IMR), Tohoku University,
2-1-1 Katahira, Aoba-ku, Sendai 980-8577, Japan*

²*Department of Material Science, University of Hyogo, Ako, Hyogo 678-1297, Japan*

³*RIKEN Center for Emergent Matter Science, 2-1 Hirosawa, Wako, Saitama 351-0198, Japan*

⁴*Department of Physics, The University of Tokyo, 7-3-1 Hongo, Bunkyo-ku, Tokyo 113-0033*

(Dated: February 21, 2025)

We explore the superconducting properties of the bilayer Hubbard model, which exhibits a high transition temperature (T_c) for an s_{\pm} pairing, using a cluster extension of the dynamical mean-field theory. Unlike the single-layer Hubbard model, where the d -wave superconductivity emerges by doping the Mott insulator, the parent state of the bilayer system is a correlated band insulator. Above T_c , slight hole (electron) doping introduces a striking dichotomy between electron and hole pockets: the electron (hole) pocket develops a pseudogap while the other becomes a nearly incipient band. We reveal that the superconductivity is driven by kinetic (potential) energy gain in the underdoped (overdoped) region. We also find a very short coherence length, for which we argue the relevance to multi-orbital physics. Our study offers crucial insights into the superconductivity in the bilayer Hubbard model potentially relevant to $\text{La}_3\text{Ni}_2\text{O}_7$.

Introduction. The problem of high- T_c superconductivity (SC) in strongly correlated electron systems is one of the central issues in condensed matter physics. The canonical model that represents high- T_c SC resulting from electron correlation effects has played a crucial role in elucidating the mechanisms of its occurrence [1]. The Hubbard model is one of the representative models, and in particular, the single-band Hubbard model on a square lattice has been extensively studied as a model representing high- T_c cuprates. To date, various approaches from weak to strong correlations have established the existence of an SC phase with d -wave symmetry near the Mott insulating phase [2–7].

Meanwhile, the bilayer Hubbard model has been studied as another canonical model for achieving high- T_c SC. In 1992, focusing on bilayer cuprates, Bulut *et al.* showed that increasing interlayer hopping could change the SC gap symmetry from d -wave to s_{\pm} -wave [8]. Since that discovery, the potential for high- T_c SC within the bilayer Hubbard model has been explored through various approaches [1, 9–20]. This issue has recently gained renewed attention in connection with elucidating the mechanisms behind the newly discovered bilayer nickelate high- T_c superconductor, $\text{La}_3\text{Ni}_2\text{O}_7$ [21]. In $\text{La}_3\text{Ni}_2\text{O}_7$, the low-energy states are composed of the $d_{x^2-y^2}$ and $d_{3z^2-r^2}$ orbitals [22, 23]. The roles these two orbitals play in SC, and whether they lead to the d -wave SC, similar to that observed in cuprates, or the s_{\pm} -wave SC, similar to that proposed for iron-based superconductors, remains an open question [24–42]. Among these studies, a scenario has been proposed where the $d_{3z^2-r^2}$ orbital plays the role of the active band, giving rise to a high- T_c s_{\pm} -wave SC through a mechanism inherent in the bilayer Hubbard model [43, 44].

Both the single-layer and bilayer Hubbard models share the common feature of realizing high- T_c SC near

half filling, but there are crucial differences concerning the insulating phase at half filling [45, 46]. In the case of the single-layer Hubbard model, the insulating phase is the Mott insulator, whereas in the bilayer Hubbard model, it is a correlated band insulator. For the electron and hole bands, the energy scale from the bottom of the band to the Fermi level is small, competing with the size of the SC gap, suggesting the presence of BEC (Bose-Einstein condensation)-like strong-coupling SC. While the instability toward SC in the normal state in the bilayer Hubbard model has been explored, more expensive calculations of the SC state itself have not been conducted so far, except for the filling dependence of the order parameter [40]. As a result, the nature of superconductivity remains poorly understood.

In this Letter, we analyzed the bilayer Hubbard model using the cellular dynamical mean field theory (cDMFT), one of the most reliable non-perturbative techniques [47, 48]. First, we calculate the condensation energy, showing that kinetic-energy-driven SC occurs near the correlated band insulating phase and that it crosses over to a potential-energy-driven one as the carrier doping increases. The transition temperature reaches its maximum just before the crossover region from kinetic to potential energy-driven SC, amounting to about 10 % of the in-plane transfer energy. Further analysis of the spectral function as a function of hole (electron) doping reveals that in the electron (hole) band, where the Fermi energy is small, a pseudogap opens above T_c , while the hole (electron) band exhibits conventional metallic behavior. We also evaluate the coherence length of SC, finding that near the correlated band insulating phase, the coherence length is only a few times the lattice constant, which is extremely short. If $\text{La}_3\text{Ni}_2\text{O}_7$ is described by the bilayer Hubbard model, this corresponds to ~ 1 nm, aligning with the fact that $\text{La}_3\text{Ni}_2\text{O}_7$ has a high crit-

ical field (H_{c2}) of ~ 100 T [21, 49].

Model and Methods. We consider the bilayer Hubbard model on the square lattice, whose Hamiltonian reads

$$\mathcal{H} = -t \sum_{\langle i,j \rangle, \alpha, \sigma} c_{\alpha i}^{\sigma \dagger} c_{\alpha j}^{\sigma} - t_{\perp} \sum_{i, \alpha \neq \alpha', \sigma} c_{\alpha i}^{\sigma \dagger} c_{\alpha' i}^{\sigma} + U \sum_{i, \alpha} n_{\alpha i}^{\uparrow} n_{\alpha i}^{\downarrow}, \quad (1)$$

where $c_{\alpha i}^{\sigma \dagger}$ ($c_{\alpha i}^{\sigma}$) creates (annihilates) an electron with spin σ at site i on the α -th layer ($\alpha = 1, 2$) and $n_{\alpha i}^{\sigma} \equiv c_{\alpha i}^{\sigma \dagger} c_{\alpha i}^{\sigma}$. t and t_{\perp} are intralayer nearest-neighbor hopping and interlayer hopping, respectively. We set $t = 1$ as the energy unit and study the case of $t_{\perp} = 2$ and $U = 8$. In this study, we focus on hole doping, but the results for electron doping can be obtained straightforwardly due to the particle-hole symmetry of the model.

We solve this model by cDMFT. We incorporate intralayer short-range correlations within the cluster size of 2×2 and the interlayer correlations. We employ the Nambu formalism to treat the SC phase. For the impurity solver, we use the continuous-time quantum Monte Carlo method with an interaction expansion [50, 51] developed in Ref. [52], which implements the submatrix update algorithm [53] to make the computation at low temperatures feasible [54].

If we take the bonding and antibonding basis, the non-interacting band dispersions $\varepsilon_{\gamma \mathbf{k}}$ for the bonding ($\gamma = B$) and antibonding ($\gamma = A$) orbitals are given by $\varepsilon_{B \mathbf{k}} = -t_{\perp} - 2t(\cos k_x + \cos k_y)$ and $\varepsilon_{A \mathbf{k}} = t_{\perp} - 2t(\cos k_x + \cos k_y)$, respectively. In this basis, the normal-state Green's function becomes diagonal and is given by $G_{\gamma \mathbf{k}}(i\omega_{\nu}) = [i\omega_{\nu} + \mu - \varepsilon_{\gamma \mathbf{k}} - \Sigma_{\gamma \mathbf{k}}(i\omega_{\nu})]^{-1}$ with the Matsubara frequency $\omega_{\nu} = (2\nu + 1)\pi T$ ($T = 1/\beta$ is the temperature), the chemical potential μ , and the self-energy $\Sigma_{\gamma \mathbf{k}}(i\omega_{\nu})$. In the SC phase, the anomalous part of the self-energy $S_{\gamma \mathbf{k}}(i\omega_{\nu})$ becomes nonzero.

In the current framework, we can directly obtain the self-energy at momenta $\mathbf{k} = (0, 0)$, $(\pi, 0)$, $(0, \pi)$, (π, π) . To infer the full momentum dependence, we employ the periodization scheme [47]. Specifically, we adopt the cumulant periodization method [55], which ensures rapid convergence of the periodized self-energy with increasing cluster size [56]. Hereafter, results for momenta other than $\mathbf{k} = (0, 0)$, $(\pi, 0)$, $(0, \pi)$, (π, π) are obtained through this periodization scheme.

Phase diagram. Figure 1(a) illustrates the doping dependence of T_c , revealing a clear dome-like shape. The maximum T_c reaches about 0.1, in consistency with previous studies with different methods [12, 15]. This value is significantly higher than $T_c^{\max} \simeq 0.05$ obtained from the 2×2 cDMFT calculation [57] for d -wave SC in the single-band Hubbard model. Notably, in the underdoped regime, the SC is driven by kinetic energy gain, indicating a strong-coupling nature [Fig. 1(b)]. As doping increases, a crossover to a potential-energy-driven mechanism occurs. The SC order parameter also exhibits a dome-like shape [Fig. 1(c)].

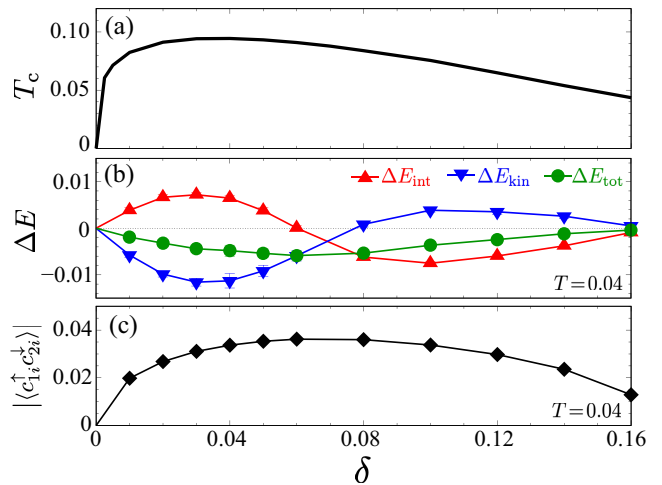


FIG. 1. Doping dependence of (a) T_c , (b) energy difference between SC and normal states at $T = 0.04$, and (c) the SC order parameter $|\langle c_{1i}^{\dagger} c_{2i}^{\dagger} \rangle|$ at $T = 0.04$.

Normal state properties. Now, we discuss how the SC emerges by investigating the normal state properties at $T = 0.1$ slightly above T_c . Figures 2(a-c), 2(d-e), 2(f-h) show the Fermi surface, effective dispersion $\xi_{\gamma \mathbf{k}}^{\text{eff}} = \varepsilon_{\gamma \mathbf{k}} + \text{Re}\Sigma_{\gamma \mathbf{k}}(0) - \mu$, and the self-energy, respectively.

In the noninteracting case, at half filling ($\delta = 0$), the system behaves as a metal with electron and hole pockets centered around $\mathbf{k} = (0, 0)$ and (π, π) , respectively. These pockets are equal in size, and hole doping reduces (increases) the size of the electron (hole) pocket.

Electron correlations, however, significantly alter this picture. At $\delta = 0$, the system transitions into an insulator due to *dynamical* band repulsion [45]. The frequency dependence of the real part of the self-energy plays a crucial role, pushing the antibonding band upward and the bonding band downward at low frequencies [Fig. 2(f)]. Upon doping, this *correlated* band insulator evolves into a metallic state. Remarkably, in the underdoped regime ($\delta = 0.02$), we do not see sharp spectral intensity for the electron pocket [Fig. 2(a)]. One might attribute this to dynamical band repulsion making the electron pocket incipient. However, the real part of the self-energy for the antibonding band bends downward at low Matsubara frequencies, counteracting the band repulsion [Fig. 2(f)]. If the imaginary part of the self-energy were neglected, the electron pocket would persist [red curve in Fig. 2(d)]. Instead, the enhancement of the imaginary part of the self-energy leads to a pseudogap in the antibonding band [Fig. 2(g)]. This suggests that the system tends to incorporate the antibonding band as an active component for SC, and the enhancement of self-energy would result from the formation of preformed pairs, as observed in the BEC regime of the attractive Hubbard model [58]. Interestingly, it is the hole pocket that becomes nearly

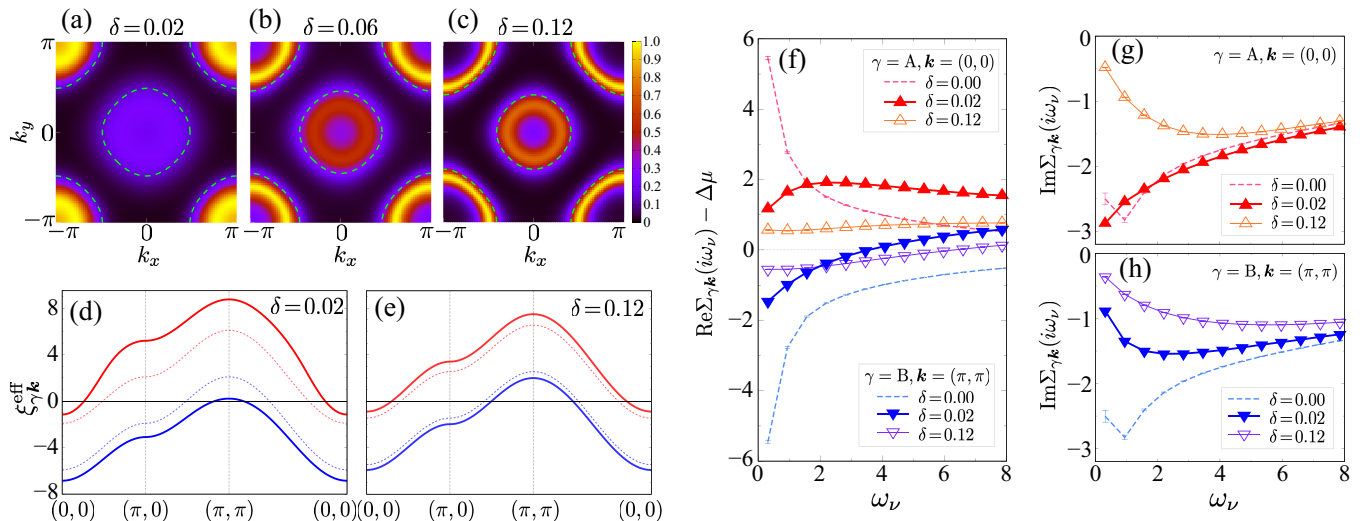


FIG. 2. The normal state properties at $T = 0.1$. (a,b,c) The Fermi surface $[-\sum_\gamma \beta G_{\gamma\mathbf{k}}(\tau = \beta/2)]$ normalized by its maximum value]. The dashed curves show the Fermi surface at $U = 0$. (d,e) The effective dispersion $\xi_{\gamma\mathbf{k}}^{\text{eff}} = \varepsilon_{\gamma\mathbf{k}} + \text{Re}\Sigma_{\gamma\mathbf{k}}(0) - \mu$ [where $\text{Re}\Sigma_{\gamma\mathbf{k}}(0)$ is approximated by $\text{Re}\Sigma_{\gamma\mathbf{k}}(i\omega_0)$]. The dotted curves show the dispersion at $U = 0$. (f) The real part of self-energy $\text{Re}\Sigma_{\gamma\mathbf{k}}(i\omega_\nu) - \Delta\mu$ for antibonding and bonding bands at $\mathbf{k} = (0,0)$ and (π,π) , respectively. $\Delta\mu$ is the change in the chemical potential between $U = 8$ and $U = 0$. (g,h) The imaginary part of self-energy $\text{Im}\Sigma_{\gamma\mathbf{k}}$ for antibonding band at $\mathbf{k} = (0,0)$ [panel (g)] and bonding band at $\mathbf{k} = (\pi,\pi)$ [panel (h)].

incipient in this regime [blue curve in Fig. 2(d)] despite doping holes. If we neglect the imaginary part of the self-energy, the size of the electron pocket is unexpectedly larger than that of the hole pocket, in stark contrast to the noninteracting case.

In the overdoped regime ($\delta = 0.12$), there are no such drastic correlation effects in the electronic structure. While the Fermi pockets are smaller than in the noninteracting case [Fig. 2(c)], this reduction can be explained by a weakly frequency-dependent, Hartree-like band shift [Figs. 2(e,f)]. Furthermore, the imaginary part of the self-energy shows Fermi-liquid-like behavior for both the bonding and antibonding bands [Figs. 2(g,h)].

Properties of SC state. Figures 3(a-c), 3(d), 3(e) illustrate the momentum dependence of the pairing amplitude, gap function, and a comparison of the self-energy between the normal and SC states, respectively. In the underdoped regime ($\delta = 0.02$), the system exhibits a strong-coupling nature. The gap function becomes large [Fig. 3(d)], reaching a magnitude comparable to the Fermi energy. As a result, the pairing amplitude distribution in momentum space broadens substantially [Fig. 3(a)], indicating the formation of localized Cooper pairs in real space. In this region, the divergence of the imaginary part of the self-energy for the antibonding band, characteristic of the pseudogap state, vanishes in the SC phase due to the emergence of coherence [Fig. 3(e)], resulting in a kinetic-energy gain. This dissolution of $\text{Im}\Sigma$ in the SC phase is similar to the behavior in the BEC regime of the attractive Hubbard

model [58]. As doping increases, the gap size decreases, and the pairing amplitude distribution becomes more concentrated around the Fermi level. This evolution of the SC state, crossing over from a BEC-like regime to a Bardeen-Cooper-Schrieffer (BCS)-like regime [59], aligns with the corresponding change of the normal state from a pseudogap regime to a conventional metallic regime.

The crossover from kinetic-energy-driven SC to potential-energy-driven SC as a function of doping is reminiscent of a similar behavior reported in previous cluster DMFT studies on the single-layer Hubbard model [57, 60, 61]. These studies demonstrated kinetic-energy-driven SC in the underdoped region, where a pseudogap forms at temperatures far above T_c . In this region, strong short-range singlet correlations above T_c limit the potential energy gain across the transition, while the emergence of coherence leads to a reduction in kinetic energy. The well-known dichotomy between antinodal and nodal regions is replaced by a dichotomy between the antibonding and bonding bands in this system. It is highly suggestive and intriguing that high- T_c SC in both single-layer and bilayer Hubbard models shares the common feature of momentum-space dichotomy in the parent normal phases. It is also interesting that the dichotomy here arises from the difference in self-energy between bonding and antibonding orbitals, making it closely related to orbital-selective physics in iron-based superconductors [62–65].

Finally, we examine the coherence length ξ of the present s_{\pm} -wave SC. For this purpose, we employ a

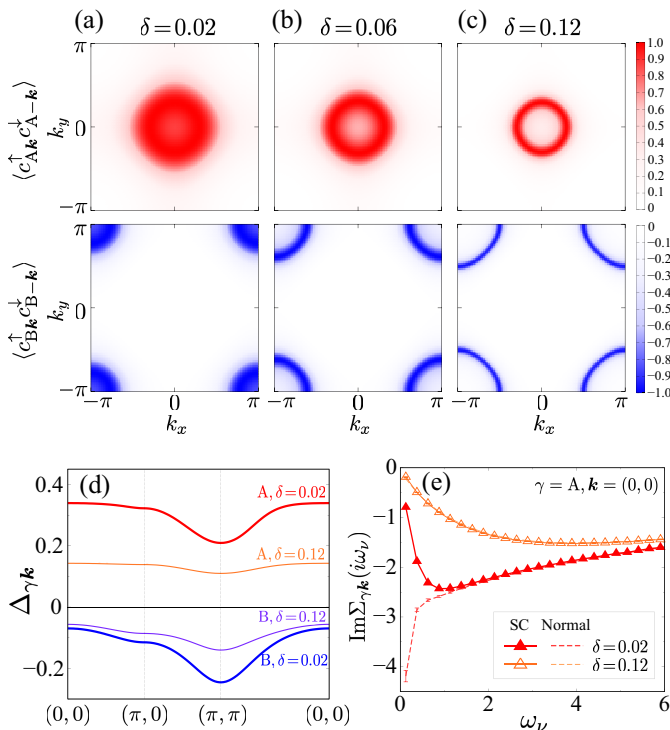


FIG. 3. The results of SC state at $T = 0.04$. (a,b,c) The pairing amplitude $\langle c_{\gamma\mathbf{k}}^\dagger c_{\gamma-\mathbf{k}}^\dagger \rangle$ in momentum space (normalized by the maximum value). (d) The SC gap function $\Delta_{\gamma\mathbf{k}}$, which is estimated from $\Delta_{\gamma\mathbf{k}} = Z_{\gamma\mathbf{k}} S_{\gamma\mathbf{k}}(i\omega_0)$ ($Z_{\gamma\mathbf{k}}$ is the quasiparticle weight). (e) Comparison of the normal part of the self-energy $\Sigma_{\gamma\mathbf{k}}(i\omega_\nu)$ between SC and normal states.

recently developed method [66]. We use $2 \times 1 \times 1$ cDMFT with an impurity problem consisting of two interlayer sites, and impose a finite-momentum pairing state by introducing an order parameter modulation of the Fulde–Ferrell type $\Psi_{\mathbf{q}}(\mathbf{r}) = |\Psi_{\mathbf{q}}| e^{i\mathbf{q}\cdot\mathbf{r}}$ [67]. From a Ginzburg–Landau expansion of the free energy, one can derive that the criterion for the disappearance of $|\Psi_{\mathbf{q}}|$ is given by $\xi|\mathbf{q}| \sim 1$. Thus, by analyzing how robust the SC is against shifts in the center-of-mass momentum of the Cooper pairs, we can estimate ξ .

Figure 4(a) displays the order parameter $\Psi_{\mathbf{q}} = \sum_{\mathbf{k}} \langle c_{1\mathbf{k}+\mathbf{q}/2}^\dagger c_{2-\mathbf{k}+\mathbf{q}/2}^\dagger \rangle$ for $\mathbf{q} = q(2\pi, 0)$, where the phase of the interlayer pairing varies along the x -direction. The results indicate a very short coherence length, on the order of a few in-plane lattice constants, consistent with the broad distribution of the pairing amplitude in momentum space [Figs. 3(a-c)]. The localized nature of Cooper pairs is also evident when compared to the behavior observed in the BCS regime of the attractive Hubbard model [dashed curve in Fig. 4(a)].

By applying the basis transformation to the bonding-antibonding basis, the bilayer Hubbard model can be mapped onto a two-orbital model [68] with an effective

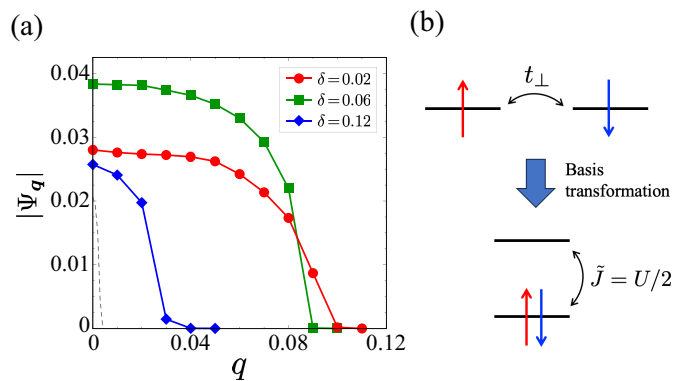


FIG. 4. (a) Order parameter of finite-momentum pairing state. The dashed curve shows the result for the single-layer attractive Hubbard model ($U = -1$) on the square lattice at half filling. (b) Mapping from the bilayer Hubbard model to an effective two-orbital model.

pair-hopping term of $U/2$ [Fig. 4(b)]. In the context of fulleride superconductors [69], it has been reported that a strong pair-hopping term significantly shortens the coherence length [66]. It would be interesting to revisit the extremely short coherence length observed in this study from the viewpoint of effective multi-orbital physics.

Discussion. If the $3d_{3z^2-r^2}$ orbital plays an active role in $\text{La}_3\text{Ni}_2\text{O}_7$, the physics discussed here should be directly relevant to high- T_c SC in $\text{La}_3\text{Ni}_2\text{O}_7$. In particular, our finding of an extremely short coherence length ξ of just a few lattice constants is highly suggestive. Given that the in-plane Ni–Ni distance in $\text{La}_3\text{Ni}_2\text{O}_7$ is approximately 3.8 \AA , our results indicate a coherence length on the order of 1 nm. This naturally explains the extraordinarily high critical field, which reaches around 100 T [21, 49]. Furthermore, it is fascinating that nickelates provide a unique platform where both single-layer physics (doped $R\text{NiO}_2$ with $R = \text{La, Pr, Nd, and Sm-Eu}$ [70–73]) and bilayer physics ($\text{La}_3\text{Ni}_2\text{O}_7$) can be explored simultaneously. This dual perspective will give a deeper understanding of high- T_c SC.

Conclusion. We have explored the nature of s_\pm -wave SC in the bilayer Hubbard model. Unlike d -wave superconductivity, which emerges from doping the Mott insulator, the SC state here arises from doping a correlated band insulator. Nevertheless, a strong momentum-space dichotomy characterized by pseudogap behavior and a crossover between kinetic-energy-driven and potential-energy-driven SC appear as common and highly suggestive features. Additionally, the connection to another high- T_c system, fullerenes, is also intriguing, as the strong effective pair-hopping term may play a crucial role in realizing SC with an extremely short coherence length ξ . Clarifying the potential relevance of this physics to $\text{La}_3\text{Ni}_2\text{O}_7$ remains a fundamentally important open question.

Acknowledgements. We acknowledge the financial support by Grant-in-Aids for Scientific Research (JSPS KAKENHI) [Grant Nos. JP23H04869 (YN), JP23H04519 (YN), JP23K03307 (YN), JP23H03817 (MK), JP24K17014 (MK), JP23H04528 (SS), JP22H00110 (RA), and JP24H00190 (RA)] and MEXT as “Program for Promoting Researches on the Supercomputer Fugaku” (Basic Science for Emergence and Functionality in Quantum Matter —Innovative Strongly-Correlated Electron Science by Integration of “Fugaku” and Frontier Experiments—) (Project ID: JPMXP1020200104). This work was supported by the RIKEN TRIP initiative (RIKEN Quantum, Advanced General Intelligence for Science Program, Many-body Electron Systems). The part of the calculations were performed at Supercomputer Center, ISSP, University of Tokyo.

* yusuke.nomura@tohoku.ac.jp

- [1] D. J. Scalapino, A common thread: The pairing interaction for unconventional superconductors, *Rev. Mod. Phys.* **84**, 1383 (2012).
- [2] T. A. Maier, M. Jarrell, T. C. Schulthess, P. R. C. Kent, and J. B. White, Systematic Study of d -Wave Superconductivity in the 2D Repulsive Hubbard Model, *Phys. Rev. Lett.* **95**, 237001 (2005).
- [3] E. Gull, O. Parcollet, and A. J. Millis, Superconductivity and the Pseudogap in the Two-Dimensional Hubbard Model, *Phys. Rev. Lett.* **110**, 216405 (2013).
- [4] T. Misawa and M. Imada, Origin of high- T_c superconductivity in doped Hubbard models and their extensions: Roles of uniform charge fluctuations, *Phys. Rev. B* **90**, 115137 (2014).
- [5] A. S. Darmawan, Y. Nomura, Y. Yamaji, and M. Imada, Stripe and superconducting order competing in the Hubbard model on a square lattice studied by a combined variational Monte Carlo and tensor network method, *Phys. Rev. B* **98**, 205132 (2018).
- [6] H.-C. Jiang and T. P. Devereaux, Superconductivity in the doped Hubbard model and its interplay with next-nearest hopping t' , *Science* **365**, 1424 (2019).
- [7] H. Xu, C.-M. Chung, M. Qin, U. Schollwöck, S. R. White, and S. Zhang, Coexistence of superconductivity with partially filled stripes in the hubbard model, *Science* **384**, eadh7691 (2024).
- [8] N. Bulut, D. J. Scalapino, and R. T. Scalettar, Nodeless d -wave pairing in a two-layer Hubbard model, *Phys. Rev. B* **45**, 5577 (1992).
- [9] S. Karakuzu, S. Johnston, and T. A. Maier, Superconductivity in the bilayer Hubbard model: Two Fermi surfaces are better than one, *Phys. Rev. B* **104**, 245109 (2021).
- [10] T. A. Maier, V. Mishra, G. Balduzzi, and D. J. Scalapino, Effective pairing interaction in a system with an incipient band, *Phys. Rev. B* **99**, 140504 (2019).
- [11] V. Mishra, D. J. Scalapino, and T. A. Maier, $s\pm$ pairing near a Lifshitz transition, *Scientific Reports* **6**, 32078 (2016).
- [12] T. A. Maier and D. J. Scalapino, Pair structure and the pairing interaction in a bilayer Hubbard model for unconventional superconductivity, *Phys. Rev. B* **84**, 180513 (2011).
- [13] N. Lanatà, P. Barone, and M. Fabrizio, Superconductivity in the doped bilayer Hubbard model, *Phys. Rev. B* **80**, 224524 (2009).
- [14] K. Bouadim, G. G. Batrouni, F. Hébert, and R. T. Scalettar, Magnetic and transport properties of a coupled Hubbard bilayer with electron and hole doping, *Phys. Rev. B* **77**, 144527 (2008).
- [15] K. Kuroki, T. Kimura, and R. Arita, High-temperature superconductivity in dimer array systems, *Phys. Rev. B* **66**, 184508 (2002).
- [16] A. I. Liechtenstein, I. I. Mazin, and O. K. Andersen, s -Wave Superconductivity from an Antiferromagnetic Spin-Fluctuation Model for Bilayer Materials, *Phys. Rev. Lett.* **74**, 2303 (1995).
- [17] R. R. dos Santos, Magnetism and pairing in Hubbard bilayers, *Phys. Rev. B* **51**, 15540 (1995).
- [18] R. E. Hetzel, W. von der Linden, and W. Hanke, Pairing correlations in a two-layer Hubbard model, *Phys. Rev. B* **50**, 4159 (1994).
- [19] R. T. Scalettar, J. W. Cannon, D. J. Scalapino, and R. L. Sugar, Magnetic and pairing correlations in coupled Hubbard planes, *Phys. Rev. B* **50**, 13419 (1994).
- [20] D. Kato and K. Kuroki, Many-variable variational Monte Carlo study of superconductivity in two-band Hubbard models with an incipient band, *Phys. Rev. Res.* **2**, 023156 (2020).
- [21] H. Sun, M. Huo, X. Hu, J. Li, Z. Liu, Y. Han, L. Tang, Z. Mao, P. Yang, B. Wang, J. Cheng, D.-X. Yao, G.-M. Zhang, and M. Wang, Signatures of superconductivity near 80 K in a nickelate under high pressure, *Nature* **621**, 493 (2023).
- [22] Z. Luo, X. Hu, M. Wang, W. Wú, and D.-X. Yao, Bilayer Two-Orbital Model of $\text{La}_3\text{Ni}_2\text{O}_7$ under Pressure, *Phys. Rev. Lett.* **131**, 126001 (2023).
- [23] V. Christiansson, F. Petocchi, and P. Werner, Correlated Electronic Structure of $\text{La}_3\text{Ni}_2\text{O}_7$ under Pressure, *Phys. Rev. Lett.* **131**, 206501 (2023).
- [24] Y. Gu, C. Le, Z. Yang, X. Wu, and J. Hu, Effective model and pairing tendency in bilayer Ni-based superconductor $\text{La}_3\text{Ni}_2\text{O}_7$, arXiv:2306.07275 [cond-mat.supr-con] (2023).
- [25] K. Jiang, Z. Wang, and F.-C. Zhang, High-Temperature Superconductivity in $\text{La}_3\text{Ni}_2\text{O}_7$, *Chinese Physics Letters* **41**, 017402 (2024).
- [26] Z. Luo, B. Lv, M. Wang, W. Wú, and D.-X. Yao, High- T_c superconductivity in $\text{La}_3\text{Ni}_2\text{O}_7$ based on the bilayer two-orbital t - J model, *npj Quantum Materials* **9**, 61 (2024).
- [27] C. Lu, Z. Pan, F. Yang, and C. Wu, Interlayer-Coupling-Driven High-Temperature Superconductivity in $\text{La}_3\text{Ni}_2\text{O}_7$ under Pressure, *Phys. Rev. Lett.* **132**, 146002 (2024).
- [28] Y. Zhang, L.-F. Lin, A. Moreo, T. A. Maier, and E. Dagotto, Structural phase transition, $s\pm$ -wave pairing, and magnetic stripe order in bilayered superconductor $\text{La}_3\text{Ni}_2\text{O}_7$ under pressure, *Nature Communications* **15**, 2470 (2024).
- [29] S. Bötzel, F. Lechermann, J. Gondolf, and I. M. Eremin, Theory of magnetic excitations in the multilayer nickelate superconductor $\text{La}_3\text{Ni}_2\text{O}_7$, *Phys. Rev. B* **109**, L180502 (2024).

- [30] F. Lechermann, J. Gondolf, S. Bötzel, and I. M. Eremin, Electronic correlations and superconducting instability in $\text{La}_3\text{Ni}_2\text{O}_7$ under high pressure, *Phys. Rev. B* **108**, L201121 (2023).
- [31] Y.-B. Liu, J.-W. Mei, F. Ye, W.-Q. Chen, and F. Yang, s^\pm -Wave Pairing and the Destructive Role of Apical-Oxygen Deficiencies in $\text{La}_3\text{Ni}_2\text{O}_7$ under Pressure, *Phys. Rev. Lett.* **131**, 236002 (2023).
- [32] G. Heier, K. Park, and S. Y. Savrasov, Competing d_{xy} and s_\pm pairing symmetries in superconducting $\text{La}_3\text{Ni}_2\text{O}_7$: LDA+FLEX calculations, *Phys. Rev. B* **109**, 104508 (2024).
- [33] Q.-G. Yang, D. Wang, and Q.-H. Wang, Possible s_\pm -wave superconductivity in $\text{La}_3\text{Ni}_2\text{O}_7$, *Phys. Rev. B* **108**, L140505 (2023).
- [34] K.-Y. Jiang, Y.-H. Cao, Q.-G. Yang, H.-Y. Lu, and Q.-H. Wang, Theory of Pressure Dependence of Superconductivity in Bilayer Nickelate $\text{La}_3\text{Ni}_2\text{O}_7$, arXiv:2409.17861 [cond-mat.supr-con] (2024).
- [35] H.-X. Xu, Y. Xie, D. Guterding, and Z. Wang, Competition of superconducting pairing symmetries in $\text{La}_3\text{Ni}_2\text{O}_7$, arXiv:2501.05254 [cond-mat.supr-con] (2025).
- [36] S. Ryee, N. Witt, and T. O. Wehling, Quenched Pair Breaking by Interlayer Correlations as a Key to Superconductivity in $\text{La}_3\text{Ni}_2\text{O}_7$, *Phys. Rev. Lett.* **133**, 096002 (2024).
- [37] Z.-Y. Shao, Y.-B. Liu, M. Liu, and F. Yang, Band Structure and Pairing Nature of $\text{La}_3\text{Ni}_2\text{O}_7$ Thin Film at Ambient Pressure, arXiv:2501.10409 [cond-mat.supr-con] (2025).
- [38] Z. Liao, L. Chen, G. Duan, Y. Wang, C. Liu, R. Yu, and Q. Si, Electron correlations and superconductivity in $\text{La}_3\text{Ni}_2\text{O}_7$ under pressure tuning, *Phys. Rev. B* **108**, 214522 (2023).
- [39] Z. Liao, Y. Wang, L. Chen, G. Duan, R. Yu, and Q. Si, Orbital-selective electron correlations in high- T_c bilayer nickelates: from a global phase diagram to implications for spectroscopy, arXiv:2412.21019 [cond-mat.supr-con] (2024).
- [40] Y.-H. Tian, Y. Chen, J.-M. Wang, R.-Q. He, and Z.-Y. Lu, Correlation effects and concomitant two-orbital s_\pm -wave superconductivity in $\text{La}_3\text{Ni}_2\text{O}_7$ under high pressure, *Phys. Rev. B* **109**, 165154 (2024).
- [41] Z. Fan, J.-F. Zhang, B. Zhan, D. Lv, X.-Y. Jiang, B. Normand, and T. Xiang, Superconductivity in nickelate and cuprate superconductors with strong bilayer coupling, *Phys. Rev. B* **110**, 024514 (2024).
- [42] L. B. Braz, G. B. Martins, and L. G. G. V. D. da Silva, Interlayer interactions in $\text{La}_3\text{Ni}_2\text{O}_7$ under pressure: from s^\pm to d_{xy} -wave superconductivity, arXiv:2502.08425 [cond-mat.supr-con] (2025).
- [43] M. Nakata, D. Ogura, H. Usui, and K. Kuroki, Finite-energy spin fluctuations as a pairing glue in systems with coexisting electron and hole bands, *Phys. Rev. B* **95**, 214509 (2017).
- [44] H. Sakakibara, N. Kitamine, M. Ochi, and K. Kuroki, Possible High T_c Superconductivity in $\text{La}_3\text{Ni}_2\text{O}_7$ under High Pressure through Manifestation of a Nearly Half-Filled Bilayer Hubbard Model, *Phys. Rev. Lett.* **132**, 106002 (2024).
- [45] S. S. Kancharla and S. Okamoto, Band insulator to Mott insulator transition in a bilayer Hubbard model, *Phys. Rev. B* **75**, 193103 (2007).
- [46] H. Lee, Y.-Z. Zhang, H. O. Jeschke, and R. Valentí, Competition between band and Mott insulators in the bilayer Hubbard model: A dynamical cluster approximation study, *Phys. Rev. B* **89**, 035139 (2014).
- [47] G. Kotliar, S. Y. Savrasov, G. Pálsson, and G. Biroli, Cellular Dynamical Mean Field Approach to Strongly Correlated Systems, *Phys. Rev. Lett.* **87**, 186401 (2001).
- [48] T. Maier, M. Jarrell, T. Pruschke, and M. H. Hettler, Quantum cluster theories, *Rev. Mod. Phys.* **77**, 1027 (2005).
- [49] F. Li, D. Peng, J. Dou, N. Guo, L. Ma, C. Liu, L. Wang, Y. Zhang, J. Luo, J. Yang, J. Zhang, W. Cai, J. Cheng, Q. Zheng, R. Zhou, Q. Zeng, X. Tao, and J. Zhang, Ambient pressure growth of bilayer nickelate single crystals with superconductivity over 90 K under high pressure, arXiv:2501.14584 [cond-mat.supr-con] (2025).
- [50] A. N. Rubtsov and A. I. Lichtenstein, Continuous-time quantum Monte Carlo method for fermions: Beyond auxiliary field framework, *Journal of Experimental and Theoretical Physics Letters* **80**, 61 (2004).
- [51] A. N. Rubtsov, V. V. Savkin, and A. I. Lichtenstein, Continuous-time quantum Monte Carlo method for fermions, *Phys. Rev. B* **72**, 035122 (2005).
- [52] Y. Nomura, S. Sakai, and R. Arita, Multiorbital cluster dynamical mean-field theory with an improved continuous-time quantum Monte Carlo algorithm, *Phys. Rev. B* **89**, 195146 (2014).
- [53] E. Gull, P. Staar, S. Fuchs, P. Nukala, M. S. Summers, T. Pruschke, T. C. Schulthess, and T. Maier, Submatrix updates for the continuous-time auxiliary-field algorithm, *Phys. Rev. B* **83**, 075122 (2011).
- [54] An open-source CT-INT program using the submatrix update as in Ref. [52] is available in Ref. [74].
- [55] T. D. Stanescu and G. Kotliar, Fermi arcs and hidden zeros of the Green function in the pseudogap state, *Phys. Rev. B* **74**, 125110 (2006).
- [56] S. Sakai, G. Sangiovanni, M. Civelli, Y. Motome, K. Held, and M. Imada, Cluster-size dependence in cellular dynamical mean-field theory, *Phys. Rev. B* **85**, 035102 (2012).
- [57] L. Fratino, P. Sémon, G. Sordi, and A. M. S. Tremblay, An organizing principle for two-dimensional strongly correlated superconductivity, *Scientific Reports* **6**, 22715 EP (2016).
- [58] S. Sakai, M. Civelli, Y. Nomura, and M. Imada, Hidden fermionic excitation in the superconductivity of the strongly attractive hubbard model, *Phys. Rev. B* **92**, 180503 (2015).
- [59] Q. Chen, Z. Wang, R. Boyack, S. Yang, and K. Levin, When superconductivity crosses over: From BCS to BEC, *Rev. Mod. Phys.* **96**, 025002 (2024).
- [60] T. A. Maier, M. Jarrell, A. Macridin, and C. Slezak, Kinetic energy driven pairing in cuprate superconductors, *Phys. Rev. Lett.* **92**, 027005 (2004).
- [61] E. Gull and A. J. Millis, Energetics of superconductivity in the two-dimensional hubbard model, *Phys. Rev. B* **86**, 241106 (2012).
- [62] T. Misawa, K. Nakamura, and M. Imada, Ab Initio Evidence for Strong Correlation Associated with Mott Proximity in Iron-Based Superconductors, *Phys. Rev. Lett.* **108**, 177007 (2012).
- [63] M. Yi, D. H. Lu, R. Yu, S. C. Riggs, J.-H. Chu, B. Lv, Z. K. Liu, M. Lu, Y.-T. Cui, M. Hashimoto, S.-K. Mo, Z. Hussain, C. W. Chu, I. R. Fisher, Q. Si, and Z.-X.

- Shen, Observation of Temperature-Induced Crossover to an Orbital-Selective Mott Phase in $A_x\text{Fe}_{2-y}\text{Se}_2$ ($A=\text{K}, \text{Rb}$) Superconductors, *Phys. Rev. Lett.* **110**, 067003 (2013).
- [64] L. de' Medici, G. Giovannetti, and M. Capone, Selective Mott Physics as a Key to Iron Superconductors, *Phys. Rev. Lett.* **112**, 177001 (2014).
- [65] M. Kim, S. Choi, W. H. Brito, and G. Kotliar, Orbital-Selective Mott Transition Effects and Nontrivial Topology of Iron Chalcogenide, *Phys. Rev. Lett.* **132**, 136504 (2024).
- [66] N. Witt, Y. Nomura, S. Brener, R. Arita, A. I. Lichtenstein, and T. O. Wehling, Bypassing the lattice BCS–BEC crossover in strongly correlated superconductors through multiorbital physics, *npj Quantum Materials* **9**, 100 (2024).
- [67] P. Fulde and R. A. Ferrell, Superconductivity in a strong spin-exchange field, *Phys. Rev.* **135**, A550 (1964).
- [68] Please refer to Ref. [75] and Supplemental Materials at http://*** for the detailed derivation for the basis transformation.
- [69] Y. Nomura, S. Sakai, M. Capone, and R. Arita, Exotic s-wave superconductivity in alkali-doped fullerides, *J. Phys.: Condens. Matter* **28**, 153001 (2016).
- [70] D. Li, K. Lee, B. Y. Wang, M. Osada, S. Crossley, H. R. Lee, Y. Cui, Y. Hikita, and H. Y. Hwang, Superconductivity in an infinite-layer nickelate, *Nature* **572**, 624 (2019).
- [71] M. Kitatani, L. Si, O. Janson, R. Arita, Z. Zhong, and K. Held, Nickelate superconductors—a renaissance of the one-band Hubbard model, *npj Quantum Materials* **5**, 59 (2020).
- [72] Y. Nomura and R. Arita, Superconductivity in infinite-layer nickelates, *Rep. Prog. Phys.* **85**, 052501 (2022).
- [73] S. L. E. Chow, Z. Luo, and A. Ariando, High-temperature Superconducting Oxide without Copper at Ambient Pressure, *arXiv:2410.00144 [cond-mat.supr-con]* (2024).
- [74] H. Shinaoka, Y. Nomura, and E. Gull, Efficient implementation of the continuous-time interaction-expansion quantum Monte Carlo method, *Comput. Phys. Commun.* **252**, 106826 (2020).
- [75] H. Shinaoka, Y. Nomura, S. Biermann, M. Troyer, and P. Werner, Negative sign problem in continuous-time quantum Monte Carlo: Optimal choice of single-particle basis for impurity problems, *Phys. Rev. B* **92**, 195126 (2015).

**Supplemental Materials for
“Strong-coupling high- T_c superconductivity in
doped correlated band insulator”**

**Yusuke Nomura, Motoharu Kitatani, Shiro Sakai,
and Ryotaro Arita**

**Mapping from the bilayer Hubbard model to an
effective two-orbital model**

The basis transformation to bonding ($c_{Bi}^\sigma = \frac{1}{\sqrt{2}}(c_{1i}^\sigma + c_{2i}^\sigma)$) and antibonding ($c_{Ai}^\sigma = \frac{1}{\sqrt{2}}(c_{1i}^\sigma - c_{2i}^\sigma)$) basis converts the bilayer Hubbard model into an effective two-orbital model. The one-body part of the Hamiltonian is transformed to

$$\mathcal{H}_0 = \sum_{\gamma=A,B} \sum_{\sigma} \varepsilon_{\gamma\mathbf{k}} c_{\gamma\mathbf{k}}^{\sigma\dagger} c_{\gamma\mathbf{k}}^{\sigma}, \quad (\text{S1})$$

where the energy dispersions are given by $\varepsilon_{A\mathbf{k}} = t_{\perp} - 2t(\cos k_x + \cos k_y)$ for the antibonding orbital ($\gamma = A$) and $\varepsilon_{B\mathbf{k}} = -t_{\perp} - 2t(\cos k_x + \cos k_y)$ for the bonding orbital ($\gamma = B$). The interaction part of the effective two-orbital Hamiltonian is given by

$$\begin{aligned} \mathcal{H}_{\text{int}} = & \tilde{U} \sum_{i,\gamma} n_{\gamma i}^{\uparrow} n_{\gamma i}^{\downarrow} + \tilde{U}' \sum_{i,\sigma} n_{Ai}^{\sigma} n_{Bi}^{-\sigma} + (\tilde{U}' - \tilde{J}) \sum_{i,\sigma} n_{Ai}^{\sigma} n_{Bi}^{\sigma} \\ & + \tilde{J} \sum_{i,\gamma \neq \gamma'} c_{\gamma i}^{\uparrow\dagger} c_{\gamma' i}^{\uparrow} c_{\gamma' i}^{\downarrow\dagger} c_{\gamma i}^{\downarrow} + \tilde{J} \sum_{i,\gamma \neq \gamma'} c_{\gamma i}^{\uparrow\dagger} c_{\gamma' i}^{\uparrow} c_{\gamma' i}^{\downarrow\dagger} c_{\gamma i}^{\downarrow}, \quad (\text{S2}) \end{aligned}$$

where the interaction parameters are defined as $\tilde{U} = \tilde{U}' = \tilde{J} = U/2$. In particular, the last term corresponds to the effective pair-hopping term depicted in Fig. 4(b), which provides a direct pairing interaction. Since the sign of this pairing interaction is positive, the phase of the pairing exhibits a sign change between the bonding and antibonding bands, leading to the pairing symmetry of s_{\pm} -wave.